CIVIL AND ENVIRONMENTAL ENGINEERING REPORTS

E-ISSN 2450-8594

CEER 2025; 35 (4): 0038-0060
DOI: 10.59440/ceer/209475
Original Research Article

ANALYSIS OF GLACIAL FRONT DYNAMICS IN HORNSUND FJORD (SVALBARD) OVER 30 YEARS USING LANDSAT MULTISPECTRAL IMAGERY

Paulina MODLIŃSKA *, Filip MRÓZ, Anna KOPEĆ
Faculty of Geoengineering, Mining and Geology, Wrocław University of Science and Technology, Wrocław, Poland

Abstract
This study investigates the long-term dynamics of glacier fronts in the Hornsund Fjord (Svalbard) over a 30-year period (1992–2023), utilizing multispectral Landsat satellite imagery in conjunction with advanced GIS-based methods. While numerous studies have examined glacial retreat using photogrammetry or field measurements, this research addresses a semi-automated approach that integrates raster segmentation and supervised classification for precise front delineation and the calculation two types of indicators of curvature of glacial front (CfD and CfE).A distinguishing feature of this study is the comprehensive temporal coverage and standardized, reproducible method for analyzing glacier front positions. This facilitates interannual comparisons and supports the classification of glacier behavior into dynamic phases. The analysis reveals substantial interglacial variability, with average annual retreat rates ranging from 12 m/year (Körberbreen) to over 79 m/year (Storbreen), emphasizing the heterogeneous response of tidewater glaciers to climatic and environmental forcing. The proposed methodology demonstrates potential for extending glaciological monitoring in remote regions and for enhancing the understanding of glacier–climate interactions.

Keywords: glacier fronts, glacial indicators, Landsat, Svalbard, multispectral imaging

1. INTRODUCTION

Glaciers, critical components of the global climate system and water resources, are undergoing dynamic geometric changes, mainly due to melting. Over the past decades, technical development has opened up new perspectives regarding the collection and analysis of glacier-related data, enabling the creation of accurate glacier maps and long-term studies of glacier length, width, thickness and ice movement

* Corresponding author: Paulina Modlińska, Wroclaw University of Science and Technology, Faculty of Geoengineering, Mining, and Geology, Department of Geodesy and Geoinformatics, Wyb. Wyspiańskiego 27, 50-370 Wrocław, Poland, e-mail: paulina.modlinska@pwr.edu.pl

velocity. It provides a large amount of valuable information on the dynamics of glaciers and their response to climate changes [1].

Traditional methods of glacier front mapping initially relied on in situ surveying techniques, such as the use of ablation stakes and photogrammetry [2] [3]. Over time, these classic surveying methods have been increasingly supported or replaced by more modern, efficient, and less time-consuming techniques—most notably GNSS-based surveys and remote sensing [4] [5]. These advancements have significantly improved the accuracy of glacier monitoring, particularly in the challenging conditions of polar environments.

Remote sensing has become an indispensable tool for monitoring glaciers, especially in vast and logistically challenging polar environments. Both active and passive satellite-based systems provide the spatial and temporal resolution necessary to conduct long-term, multi-glacier analyses with consistent methodology.

While LiDAR (Light Detection and Ranging) provides extremely high-resolution data for generating Digital Elevation Models (DEMs), its use is typically limited to local-scale studies and requires airborne platforms. Jóhannesson et al. [6] showed that LiDAR-derived DEMs can deliver precise surface elevation data useful for analyzing surface morphology and periglacial areas, though these campaigns are often constrained by cost, logistics, and weather conditions.

Among active remote sensing technologies, Synthetic Aperture Radar (SAR) has become one of the most versatile tools for glacier monitoring, particularly in polar regions. Its ability to acquire data regardless of cloud cover and lighting conditions makes it uniquely suited to year-round observations in the Arctic and Antarctic, where optical data are often limited by poor weather and long periods of darkness [7] [8]. SAR data are widely used for measuring ice surface velocity, frontal retreat/advance, surface deformation, and mass balance.

Glaciological studies commonly employ two main active remote sensing techniques. The first is interferometric synthetic aperture radar (InSAR), which detects centimeter-scale vertical or horizontal surface displacements by analyzing phase differences between radar images. The second is offset tracking, which estimates glacier displacement by tracking the movement of distinguishable surface features—such as crevasses, debris, or texture patterns—across sequential satellite images [9] [10]. For example, Friedl et al. [11] successfully applied Sentinel-1 offset tracking to map frontal changes of tidewater glaciers in Svalbard, providing monthly records of front fluctuations and flow speed.

Complementing these active radar-based methods, multispectral imaging has also been widely applied to assess glacier behavior, particularly in monitoring changes in ice cover, surface albedo, melt patterns, and the presence of supraglacial features [12] [13]. This technique leverages the spectral properties of snow, ice, and meltwater to disting. Suish between different surface types and monitor temporal variations. For instance, Arigony-Neto et al. [14] used multispectral satellite imagery to monitor glacier changes on the Antarctic Peninsula, emphasizing variations in ice extent and melt-related processes over time. Similarly, Paul et al. [15] demonstrated the effectiveness of Landsat TM data for mapping glacier outlines and detecting retreat in the Swiss Alps. Moreover, multispectral data have been instrumental in generating glacier inventories and detecting long-term trends in glacial retreat, especially in remote or inaccessible areas. The spectral contrast between clean ice, debris-covered ice, and meltwater enables researchers to track surface evolution and interpret climatic influences on glacier behavior [16] [17]. These capabilities make multispectral imaging a fundamental tool in large-scale, long-term glacier monitoring efforts.

Although a substantial number of regional and global studies have examined glacier front dynamics using both optical and radar satellite data [18] [19], many of them aim to capture broad spatial trends. In contrast, there remains a relative scarcity of long-term, spatially explicit analyses conducted at the scale of entire fjord systems that apply a consistent and repeatable methodological framework.

Existing research frequently focuses on individual glaciers [20] [21], covers limited timeframes [8] [22] or relied on manually interpreted data [23] [24], which has hindered the comparability of results.

This study attempts to address this gap by proposing an approach that utilizes Landsat satellite imagery, GIS techniques, and specific indicators (CfD and CfE). This enables a consistent, quantitative assessment of glacier front dynamics across the entire Hornsund fjord over the past 30 years.

2. STUDY AREA

The Svalbard Archipelago is located entirely within the Arctic Ocean, bordered by the Greenland Sea to the west, the Barents Sea to the east, and the Arctic Basin to the north. It spans latitudes 76.5°N to 80.8°N and longitudes 10°E to 34°E, lying approximately 800 km from mainland Europe and 1,100 km from the North Pole. Comprising about 150 islands and covering 62,248 km², its largest island, Spitsbergen, features Hornsund Fjord - the southernmost bay of the archipelago, shaped by glacial activity (Fig. 1).

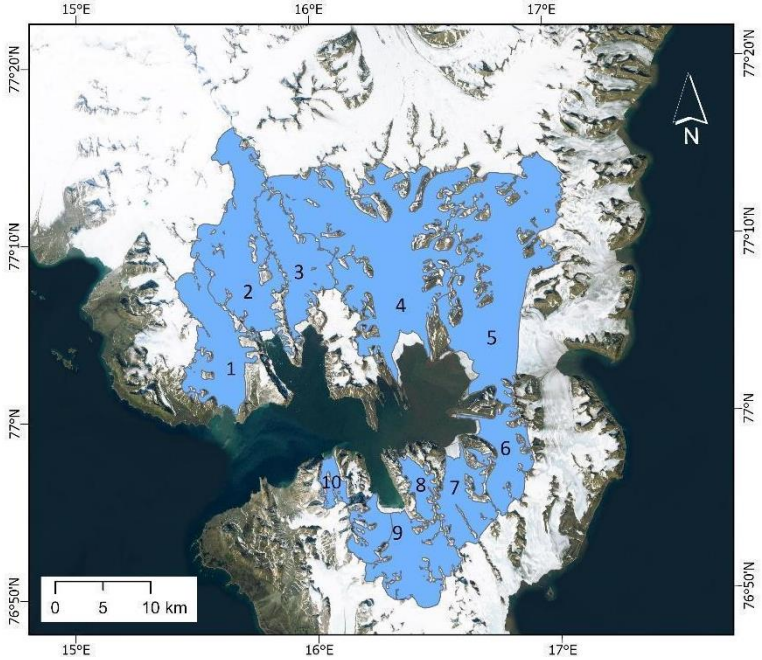

Fig. 1. Study area - the glaciers area has been marked in blue. The location of individual glaciers on the map is summarised in Tab. 1

The glaciological characteristics of Svalbard are shaped by the presence of over 2,000 glaciers of various types. Large, continuous ice sheets dominate the region, while cirque glaciers are primarily found near mountainous terrain and nunataks. In the warmer coastal areas, tidewater glaciers prevail, forming a nearly 1,000-km-long ice-sea interface [25]. Within Hornsund Fjord, often classified as a fjord due to its glacial origin, 14 glaciers terminate directly into the fjord waters, contributing to approximately two-thirds of its hydrological drainage area. The fjord itself extends 30 km in length and reaches up to 12 km in width [26]. Tab. 1 summarizes key characteristics of 10 Hornsund's glaciers selected for analysis.

Table. 1. Characteristics of the glaciers selected for analysis, based on National Snow and Ice Data Center - glacier inventory: http://nsidc.org/data/glacier_inventory

		Total area [km²]	Average height [m]	Class
1	Hansbreen	64.0	350	5
2	Paierlbreen	112.0	400	5
3	Mühlbacherbreen	56.6	420	5
4	Storbreen	238.0	280	5
5	Hornbreen	179.0	290	4
6	Svalisbreen	44.0	260	5
7	Mendeleevbreen	45.0	250	5
8	Chomjakovbreen	15.1	300	5
9	Samarinbreen	81.0	300	5
10	Körberbreen	11.4	270	5

Despite its relatively small area, Hornsund features a highly indented coastline formed by five secondary bays: Vestre and Austre Burgerbukta, Samarinvågen, Adriabukta, and Brepollen—the latter being the easternmost and youngest, created in the early 20th century due to the retreat of the Hornbreen glacier [23] [27]. Since 1936, the fjord's surface area has increased from approximately 188 km² to 311 km² by 2013 [27]. This corresponds to an average area growth rate of about 1.6 km² per year. However, the rate of retreat accelerated in the early 21st century, with estimates indicating an increase to approximately 3 km² per year between 2001 and 2010 [23]. Projections suggest that the fjord could eventually evolve into a strait connecting the Greenland and Barents Seas [28].

Climatically, Hornsund lies within the Arctic marine climate zone, characterized by relatively mild temperatures due to the influence of the West Spitsbergen Current, which brings warm Atlantic waters into the fjord from the southeast. This current plays a crucial role in modulating the local climate and salinity levels, as well as in transporting Arctic sea ice.

Meteorological observations have been conducted at the Polish Polar Station Hornsund (*pl. Polska Stacja Polarna Hornsund*, PSP Hornsund), located in the northwestern part of the fjord, since 1979. The average annual air temperature between 1979 and 2015 was -4.0°C. Annual precipitation ranged from 230 mm (1987) to 638 mm (2006), with a mean value of 433 mm. Notably, a warming trend has been recorded, with temperatures increasing by 1.14°C per decade. This rate is strikingly high when compared to the global average warming rate, which has been approximately 0.18°C per decade [29]. Thus, the warming observed in Hornsund is over six times faster than the global mean, emphasizing the pronounced effects of Arctic amplification—where processes such as sea ice loss, reduced surface albedo, and changes in atmospheric dynamics intensify warming in polar regions relative to the global average. This warming is accompanied by an increase in the number and duration of melt days, which now average 39.1 days per year, with significant growth in frequency since 2000 [30]. From a hydrological perspective, freshwater input into the Hornsund Fjord has markedly increased in recent decades. According to Błaszczyk et al. [31], the average freshwater discharge between 2006 and 2015 amounted to 2,517 Mt ± 82 per year, derived primarily from glacier meltwater. All sources of a freshwater input to the Hornsund Fjord are summarized in Tab. 2.

Table. 2. The sources and distribution of freshwater input to the Hornsund Fjord from 2006 to 2015 by Błaszczyk et al. (2019)

Meltwater glacier runoff	39%
Calving of glacier fronts	25%
Precipitation on land excluding snow	21%
Snowmelt	8%
Precipitation on the fjord	7%

In summary, the Hornsund region represents a complex and dynamic Arctic environment shaped by unique geological structures, diverse glacier systems, and rapidly evolving climatic and hydrological conditions. The region's sensitivity to climate change is evidenced by observable trends such as glacier retreat, increasing temperatures, and growing freshwater input. These interconnected processes make Hornsund a valuable area for multidisciplinary scientific research on Arctic change.

3. METHODOLOGY

With advancements in technology, remote sensing measurements have become essential tools in geographic and environmental research. They enable large-scale monitoring of environmental changes without relying on traditional, complex, and time-consuming field measurements. Remote data acquisition, using both active and passive sensors, allows for efficient and comprehensive information collection, particularly valuable for glacier studies. These techniques facilitate the monitoring of changes in glacier geometry and their temporal fluctuations.

A variety of methods, such as spectral indices (e.g., Normalized Difference Snow Index - NDSI), raster segmentation, and satellite image classification, have been employed to analyze these changes. These approaches support the identification of glacier fronts and enable the tracking of their shifts over time through glacial indices.

3.1. Front extraction - segmentation

Spectral indices, which leverage specific channels characteristic of the area under study, provide an effective means of identifying changes in glacier geometry. The NDSI, calculated from the visible (typically GREEN) and shortwave infrared (SWIR) bands, is widely used for glacier monitoring. This index is based on the unique spectral properties of ice and snow—namely, high reflectance in the visible range and distinct absorption in the SWIR range.

Snow and ice are identified using observations at two specific wavelengths: 0.66 μm and 1.6 μm. At these wavelengths, atmospheric transparency enables light penetration, allowing precise measurements. Snow exhibits a characteristic behavior: it strongly reflects light in the visible range (e.g., 0.66 μm) but absorbs it almost entirely in the near-infrared range (e.g., 1.6 μm). Conversely, clouds are highly reflective in both ranges, enabling the NDSI to effectively distinguish between clouds and snow or ice in multispectral images [32] [33].

$$NDSI = \frac{GREEN - SWIR}{GREEN + SWIR} \tag{3.1}$$

Raster segmentation refers to the process of grouping individual pixels into larger, homogeneous units (segments) based on specified criteria, with the goal of minimizing internal variability within each

segment. Before merging two segments, it is crucial to verify that the operation will not introduce excessive heterogeneity; otherwise, the segments should remain separate. Segmentation process should fulfill the following conditions:

- Complete spatial coverage of the analysis area, ensuring every pixel is assigned to a segment;
- Topological validity, with no overlaps or intersections between segments;
- Internal consistency within segments, based on common characteristics such as spectral values or texture;
- Distinctiveness between segments, allowing clear differentiation based on user-defined features;
- Compliance with user-defined thresholds, where segment attributes fall within specified parameter ranges [34].

The two additional methods of classification include unsupervised and supervised classification. Unsupervised classification involves the automatic grouping of pixels into clusters based on their spectral characteristics. These clusters are subsequently defined and associated with specific terrain representations. In this approach, pixels are assigned to spectral classes by an algorithm without prior knowledge of their field characteristics. One of the most widely used algorithms for this method is K-means clustering [35]. This algorithm groups pixels by brightness similarity, refining clusters iteratively by updating centroids and reassigning pixels. A key limitation is that clusters may mix pixels from different classes, making classification ambiguous. Thus, it works best for simple, distinct land cover types [36].

In contrast, supervised classification focuses on isolating predefined field classes. In this procedure, training fields, representing spectral patterns for each class, are created by the user. Accurate selection of these training fields is critical to ensuring they reflect the spectral characteristics of all categories. The spectral resolution of the identified classes plays a significant role in determining the accuracy of the classification. Several algorithms are commonly employed for supervised classification, including Parallelepiped Classification, Minimum Distance Classification (MDC), Mahalanobis Distance Classification, Support Vector Machine (SVM), Random Forest (RF), and Maximum Likelihood Classification (MLC) [35] [37] [38].

3.2. Glacial front indicators

Glaciers draining into Hornsund Fjord are characterized by significant and rapid variations in their features. This variability is strongly influenced by meteorological, hydrological, and climatic factors. With the availability of high temporal resolution satellite data, it is now possible to conduct comprehensive studies of the geometric changes of glacial fronts.

Fronts represent the least stable parts of glaciers due to their close proximity to water bodies, their susceptibility to currents, and the calving process—the breaking off of glacial blocks, a phenomenon exclusive to this part of the glacier. While the position of the front is the most prominent and widely recognized factor in studies investigating the melting of glacial masses, it is not the sole determinant of how glaciers respond to the aforementioned factors.

As part of research into the phenomenon of glacial surges—the sudden advance of glacial masses—indicators of glacial fronts have been developed [39]. These indicators are based on four geometric parameters of the front: the length of the front line (*Lc*), the straight-line distance between the two tangent points where the glacier meets the surrounding valley (*Dc*), the area of the circle formed by rotating the *Dc* line (*Ac*), and the area between the glacier front line (*Lc*) and the edge of the *Ac* circle (*Ag*) (Fig. 2).

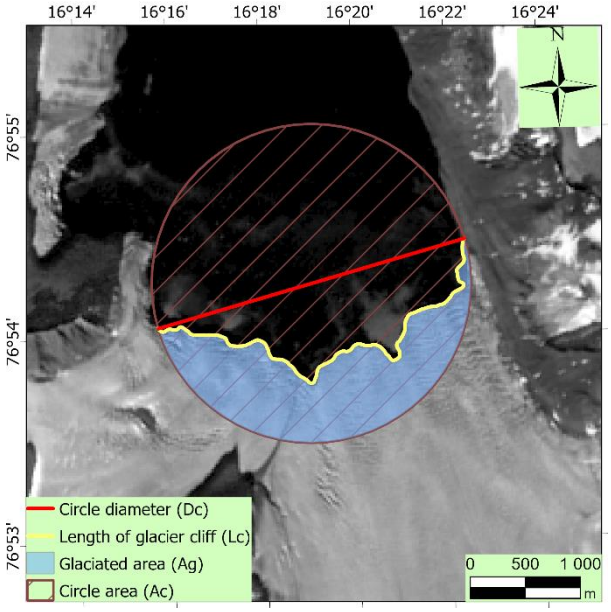

Fig. 2. Glacier indicators visualisation. Background represents the northern part of Samarinbreen glacier via 8A Sentinel-2 band. EPSG:32633

These parameters are used to determine two key indicators: glacier front dynamics, *CfD = Ag/Ac*, and the ice-cliff balance indicator, *CfE = Dc/Lc*. The *CfD* index quantifies the curvature of the glacial front, typically within the range (0,1). A value of 0 signifies a deep glacier recession extending beyond the virtual boundary defined by the Ac parameter, resulting in a concave curvature. A value of 0.5 represents an equilibrium state, also referred to as stagnation, where the curvature is minimal. A value of 1 indicates a convex curvature, which likely corresponds to a pronounced advance of the glacier front. In some cases, *CfD* values may exceed 1, indicating an extension beyond the *Ac* area. The *CfE* index examines the balance between the length of the front line and the distance between the tangent points of the valley, providing insights into the curvature of the glacial front. *CfE* values are also generally within the range (0,1). A value near 0 reflects a significant imbalance between *Dc* and *Lc*, indicative of either a deep recession or an advance of the valley glacier. Although identical CfE values may arise from both advancing and retreating glacier fronts, a sign convention is adopted to distinguish between these two behaviors: negative (–) values denote retreat, while positive (+) values indicate advance. In the present study, CfE values are reported as unsigned absolute magnitudes for clarity and consistency. The sign convention is applied solely for descriptive purposes and does not serve a mathematical function in data processing. When *CfE* approaches 1, the parameters converge, indicating glacier front stagnation. The development of these indices enabled the authors to classify glaciers terminating in water into five categories, based on changes in the respective indices between measurement periods (*ΔCfD* and *ΔCfE*). This classification is presented in Tab. 3 [39]. Other indicators are also used in the literature to quantitatively characterize glacier frontal ablation processes. Examples include such parameters as *calving extent ratio (CER*) and *calving interval index (Cii*). The *CER ratio* determines the percentage of the length of an ice cliff covered by calving episodes relative to its total length, making it possible to assess the spatial extent of calving activity on specific days of the study period. The *Cii index*, in turn, is defined as the number of days without recorded calving episodes at a given glacier front location in 10-day intervals. It is calculated as an average value for the entire front and separately for the highlighted sectors, providing information on the average duration of gaps between calving events [24].

Table. 3. Classification of glacier dynamics phases based on *ΔCfD* and *ΔCfE* indicators (Szafraniec, 2020)

Class	*ΔCfD* (interannual)	*ΔCfE* (interannual)
Advance (active phase of surge)	0-0.2	0-0.2
Filling the frontal zone	-0.2-0	0-0.2
Stagnation	~0	~0
Retreat (quescient phase of surge)	-0.2-0	-0.2-0
Deep recession	0-0.2	-0.2-0

In the approach described above, the outlines of glacial fronts were manually vectorized. This study aims to identify the most efficient method for automating the extraction of glacial fronts and subsequently calculating glacial indices.

4. SELECTION OF THE EXTRACTION METHOD

Changes in the geometry of frontal positions were analyzed for ten glaciers located in Hornsund Fjord. The temporal analysis focused on the summer and early autumn months (July to September) between 1992 and 2023, as the polar night occurs from 26 October to 16 February. Parameters such as cloud cover, satellite type, glacier visibility, and observation time were considered for image selection. A total of 11 multispectral images from the Landsat 5, 7, 8, and 9 missions were selected (see Tab. 4).

A key advantage of Landsat data is its multispectral nature, offering multiple spectral bands. This makes it possible to distinguish in more detail the surface coverage of the study area by glacial ice, snow, meltwater, debris, and allows the use of various spectral indices (e.g., NDSI, NDWI) and classification techniques. In contrast, Synthetic Aperture Radar (SAR) data are very useful because they can capture images in all weather conditions and both day and night. However, SAR usually provides only a single-band amplitude or coherence signal. This limits its ability to differentiate surface types based on spectral reflectance. As a result, accurate classification is more difficult without extensive preprocessing or additional data.

Table 4. Multispectral images used to analyze changes in glacier frontal position geometry

Satelite	Date of acquisition (note: not in order)	Data processing level	Bands	Spectral band resolution [m]
LT05	24.07.1992	L1	B1, B2, B3, B4, B5, B6[2], B7	30
LT05	03.09.1995			
LT05	27.07.1999			
LT05	14.08.2006			
LE07	12.07.2002		B1, B2, B3, B4, B5, B6 - VCID1, B6 - VCID2[3], B7	30
LE07	11.09.2010[4]			
			B8	15
LC08	24.08.2013		B1, B2, B3, B4, B5, B6, B7	30
LC08	06.07.2015			
LC08	19.08.2017			
LC08	18.08.2019			
LC08	11.07.2021		B8	15
LC09	22.09.2023		B9, B10*, B11[5]	30

Segmentation is often a preliminary step to classification, but in this case, it was used as a separate method to determine the geometry of glaciers. The *Segment Mean Shift* tool (ArcGIS Pro) was used, with its algorithm grouping neighbouring pixels into segments with similar spectral characteristics. 8-bit image stacks consisting of channels 3, 2, and 1 were created and subjected to radiometric and atmospheric correction. Parameters were selected individually for each image; these included the spectral detail value, spatial detail value, and the minimum dimension of the segment to be mapped. For the first attribute, values between 0 and 20 were selected, with a higher value indicating a higher sensitivity to feature similarity, leading to an expansion in the number of segmentation clusters. For the second parameter, the range of value choices was identical, but segments reaching values above a user-set threshold were divided into smaller ones. Several tests were required to obtain an optimal result that precisely defined the geometry of the glaciers. An exception was made in the 2002 imaging, for which

[2] The spatial resolution for the B6 (L5) thermal channel is 120 m

[3] The spatial resolution for the B6 (L7) thermal channel is 60 m

[4] The Hansbreen could not be analysed for this date due to extremely intense and extensive cloud cover. Therefore, it was decided to exclude the 2010 data for this glacier in the further stages of the analysis

[5] The spatial resolution for the B10 and B11(L8/9) channel is 100 m, however, the Earth Explorer service provides data resampled to 30 m

two segmentation iterations were performed due to the ambiguous separation of the Hornbreen glacier. Tab. 5 summarises the parameter values selected for the segmentation operation for each glacier. The first stage of data processing is visualised in Fig. 3.

Table 5. Multispectral images used to analyze changes in glacier frontal position geometry

Year	Spectral Detail	Spatial Detail	Minimum Segment Size
1992	18	18	20
1995	18.5	18	20
1999	19	19	20
2002	15.5	15	20
2002 (parameters for Hornbreen Glacier)	20	20	20
2006	19	5	15
2010	19	19	20
2013	20	20	20
2015	15.5	15	20
2017	15.5	15	20
2019	15.5	15	20
2021	10	10	20
2023	19	19	20

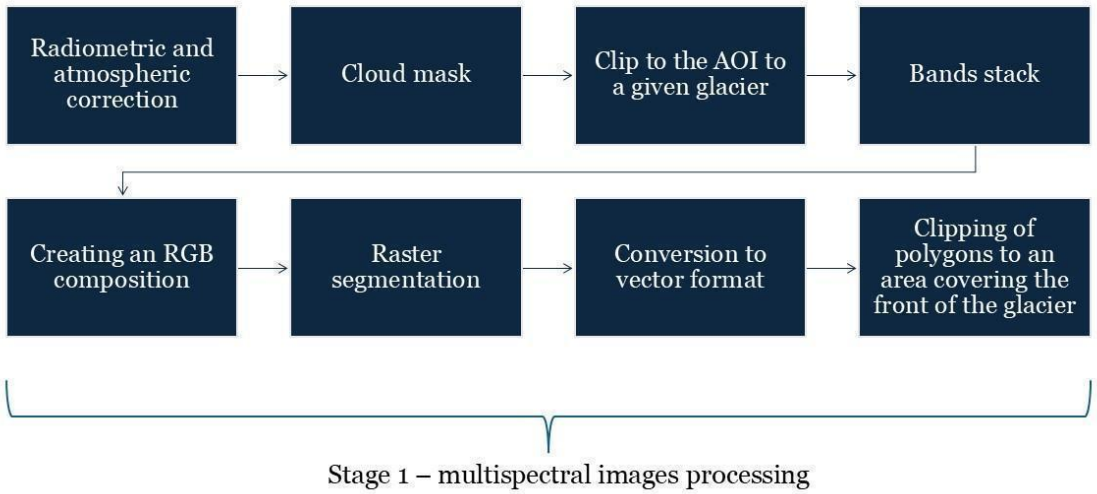

Fig. 3. Diagram of the first stage of data processing

The segmentation procedure served as the foundation for generating the polygons defining the geometry of the glaciers; however, further processing of these elements was required to obtain the frontal course. This process was automated using Python programming language code. The specific stages are presented in Fig. 4 and described below.

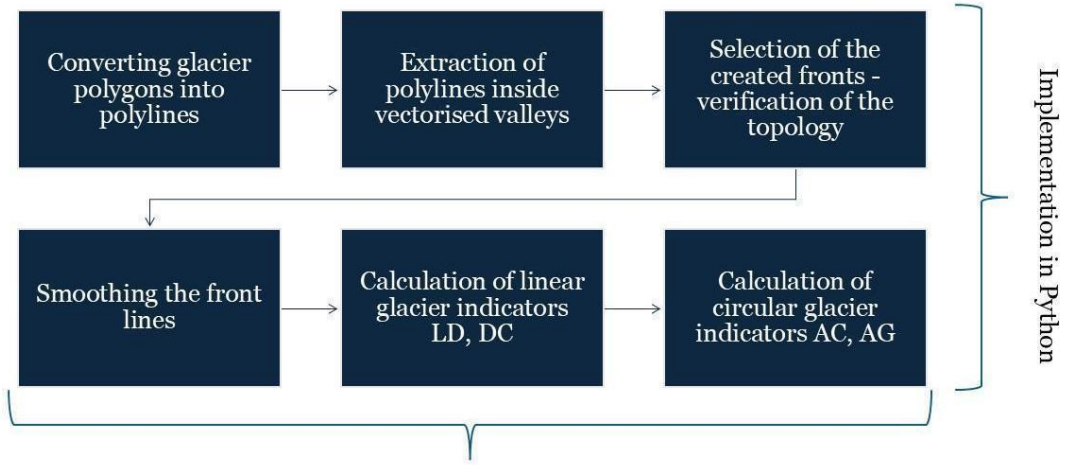

Fig. 4. The second stage of processing- implementation in the Python environment

After segmentation, the resulting polygons were converted into polylines for each year. However, since segmentation relies solely on spectral similarity, it sometimes misidentified lateral glacial moraines and other complex boundary features. To address this limitation, supervised classification using was applied, allowing for the accurate separation of ice, water, and land (Fig.5). Supervised classification was performed on the earliest (1992) and the most recent (2023) images, while also verifying and adjusting the glacier outlines for the intervening years when necessary. This refinement step allowed for a more accurate representation of glacial geometry over time. In this study, three supervised classification methods were tested: Maximum Likelihood Classification (MLC), Support Vector Machine (SVM), and Random Forest (RF).

- MLC is a parametric method that assumes normally distributed classes and performs reliably with multispectral data, especially when training data are limited [40].
- SVM is a non-parametric method that is effective with high-dimensional data and maintains high accuracy even with a small number of samples, but nevertheless requires fine-tuning of parameters [41]
- RF is a classification method that combines many decision trees to improve accuracy. It performs well with complex data and is resistant to errors, though it requires more computing power and the results can be harder to explain [42]

Among the tested methods, MLC proved to be the most suitable for the study area due to its capacity to minimize shadow effects and provide standardized outputs. An example of the classification accuracy (error matrix) for the 2002 image is presented in Table 6.

The integration of segmentation and supervised classification resulted in input polygons delineating glacial valleys, within which glacier fronts were systematically extracted.

In the initial stages of glacial front delineation, manual vectorization was employed due to its precision and the need to validate the methodology. However, with the growing volume of satellite data spanning over 30 years, fully manual processing became increasingly time-consuming and potentially subject to user bias. Therefore, the transition towards semi-automated and automated approaches, such as supervised classification and segmentation, allowed for a more efficient workflow. The combination of both approaches enabled us to maintain high-quality outputs while scaling up the temporal analysis.

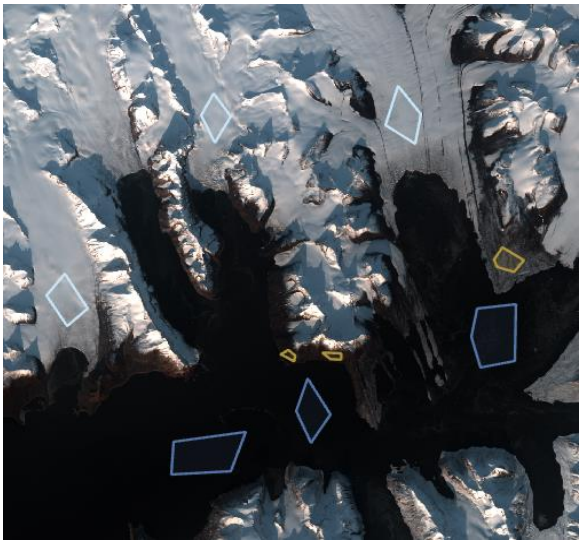

Fig. 5. Generating training fields for three class: ice, water, ground

Table 6. An example of the post-classification error matrix for the 2002 imaging for MCL method

Class	Ice	Land	Water	Total	User Accuracy	Kappa Coefficient
Ice	9	0	0	9	1	0
Land	0	6	2	8	75%	0
Water	0	0	8	8	100%	0
Total	10	6	10	30	0	0
User Accuracy	90%	100%	80%	0	90%	0
Kappa Coefficient	0	0	0	0	0	0,87

The final step involved determining glacial indices based on the input products generated. Two glacier indices, CfD and CfE, were computed for 10 glaciers in the Hornsund Fjord area to quantify the extent of glacier front retreat or advance over a 20-year period, with measurements taken every two years.

The script is developed primarily using ArcPy, the native Python library using 3.1.1 version of ArcGIS Pro software, with extensive use of the UpdateCursor for editing feature attributes directly [43]. This allows for geometry-based calculations and real-time updates to spatial datasets. For each vectorized glacier front, Lc is computed using the built-in line length property, while Dc is calculated as the Euclidean distance between the front's endpoints based on XY coordinate differences. To compute Ac, the midpoint of the Dc segment is determined and used as the center of a circular buffer,

with a radius equal to half of Dc, generated via the Shapely library. The buffer's area is then calculated. Layers containing Lc, Dc, and Ac are saved into separate directories to maintain a structured output. The more complex task of deriving Ag is handled by converting buffer and front geometries into lines, creating intersected polygons, and identifying the glacier-covered portion using a spatial selection based on auxiliary point layers. In the final analytical stage, the script computes the CfD and CfE indices within ArcGIS Pro, writing the results to new attribute fields. Once all values are assigned, the script aggregates the outputs from the relevant directories and exports them to a consolidated Excel file. The exported data include key parameters and associated metadata such as source filenames and glacier identifiers, enabling further analysis outside the GIS environment.

5. RESULTS

As a result of the conducted analyses, glacier fronts were identified, and the *CfD* and *CfE* indicators were calculated. Both methods enabled the determination of the dynamics of changes and the structural features of the glaciers over the assumed time interval. Further details regarding the rate and nature of changes in individual glaciers are discussed below. The changes in the course of glacial fronts are shown in Fig. 6, and they highlight some key differences in the geometry of individual glaciers. In addition, Tab. 7 summarises the approximate annual changes (increments or retreats) in the position of the glacier front line. The average annual rate of retreat of glacier fronts in the period 1992-2023 ranged from about 12 m/year (Körberbreen) to as much as more than 79 m/year (Storbreen). We identified a clear increase in the rate of glacier retreat in the later periods, especially in 2015-2023, indicating that glacier degradation processes are accelerating.

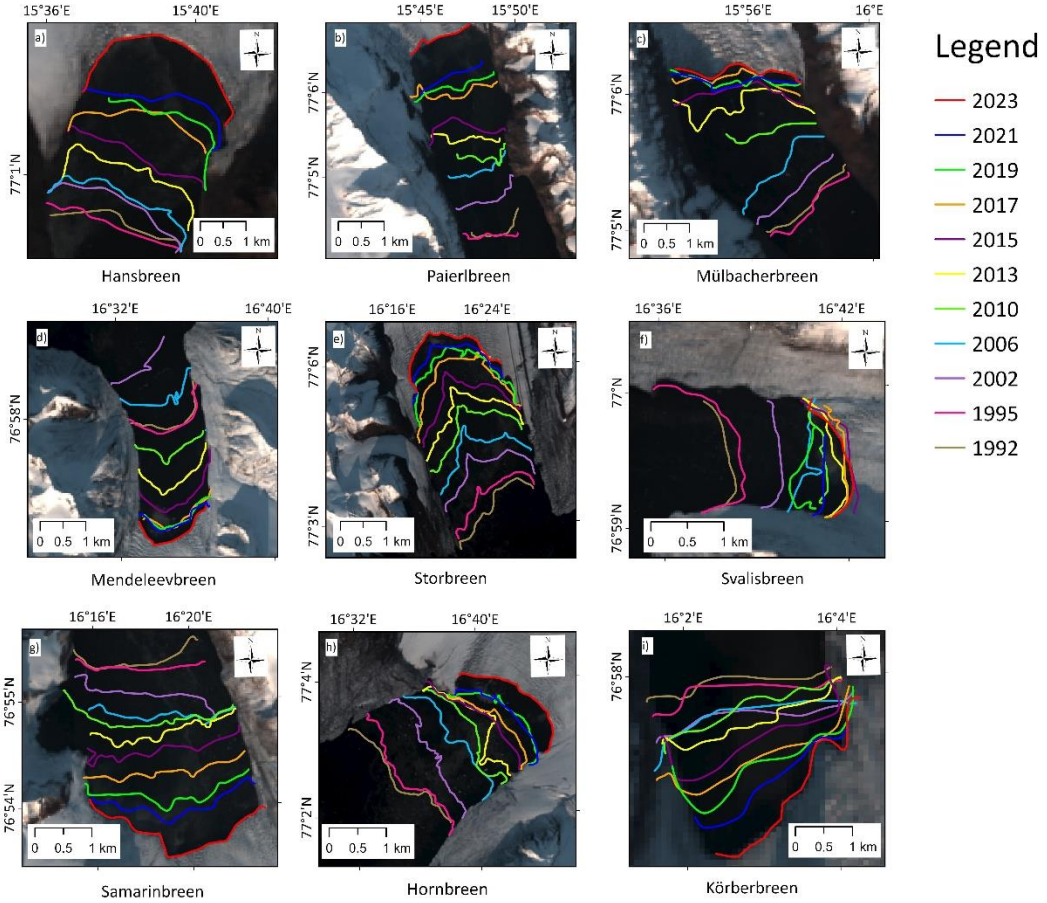

Fig. 6. Changes in the course of glacial fronts from 1992 to 2023

An analysis of glacier front position changes revealed distinct patterns of behavior across the studied glaciers, allowing for classification into three main categories based on the intensity and consistency of retreat: rapid retreaters, moderate retreaters, and stable or mildly retreating glaciers.

Rapid retreaters glaciers, including Hansbreen, Paierlbreen, and Storbreen, exhibit the highest retreat rates and the most pronounced morphological changes in their frontal zones. Hansbreen (Fig. 6a) showed the most significant retreat during the periods 2015–2017 and 2021–2023, with retreat rates of approximately 260 and 365 meters per year, respectively. In 2013, the glacier front exhibited a distinctly curved and irregular shape, likely influenced by seasonal meteorological variability or internal factors such as crevasse formation and subglacial water flow. A localized advance of the glacier was observed in its western and central sectors, approaching the extent recorded in 2002–2006. However, beyond this episode, the retreat trend remained consistent over time. Paierlbreen (Fig. 6b) began retreating notably after 1995, especially in the area adjacent to the eastern lateral moraine. As with Hansbreen, the most substantial retreat occurred between 2015–2017 and 2021–2023, with retreat rates of approximately 500 and 425 meters per year, respectively. Storbreen (Fig. 6e) demonstrated a continuous and intense retreat throughout the observation period. Since 2002, the glacier front has developed an increasingly concave shape, indicative of sustained frontal loss. Among the studied glaciers, Storbreen recorded the greatest cumulative retreat, totaling approximately 6.7 kilometers.

The moderate retreaters category includes glaciers that also exhibit retreat, though with lower intensity and greater variability over time. Glaciers such as Mühlbacherbreen, Hornbreen, and Svalisbreen are representative of this group. Mühlbacherbreen (Fig. 6c) has been undergoing notable retreat since 2010, particularly along its western lateral moraine. The greatest loss occurred between 2006 and 2013. In 2010, the shape of the glacier front changed considerably, possibly due to obstacles in the valley such as boulders or bedrock outcrops, which may have slowed ice flow and contributed to irregular frontal movement. Between 2015 and 2023, the glacier exhibited dynamic behavior with alternating periods of minor retreat and short-term advances. Hornbreen (Fig. 6h) retreated at an average rate of about 200 meters per year. A notable exception occurred between 2019 and 2021, when a brief frontal advance of approximately 75 meters per year was recorded, suggesting a temporary shift in glaciological or climatic conditions. Svalisbreen (Fig. 6f) experienced relatively rapid retreat in the early years of observation. However, between 2015 and 2019, an advance of the glacier front was noted, indicating a temporary reversal possibly driven by short-term environmental changes.

Stable or mildly retreating glaciers including Samarinbreen, Körberbreen, and Mendeleevbreen, demonstrated relatively stable front positions or slow, steady retreat. In some cases, localized advances were also documented. Samarinbreen (Fig. 6g) showed a notable narrowing of the glacier valley's western part beginning in 2019. This glacier appears to respond less dynamically to seasonal climatic variations, with only minimal fluctuations in its frontal geometry. Unlike glaciers characterized by cycles of rapid advance and retreat, Samarinbreen has exhibited a steady and gradual withdrawal. Körberbreen (Fig. 6i) is the slowest-retreating glacier among those studied, with total retreat measuring less than one kilometer. A minor frontal advance was recorded between 2002 and 2010, further illustrating its subdued response to environmental forcing. Mendeleevbreen (Fig. 6d) generally displayed moderate movement, yet a significant advance occurred between 1995 and 2002, with an average rate exceeding 200 meters per year. Since then, its retreat has been relatively mild, distinguishing it from more dynamic glacier systems in the study.

Table 7. Glacier fronts dynamics from 1992 to 2023

Glacier	Total retreat 1992 -2023 [m]	Average annual glacier front changes [m]										
		1992-1995	1995-2002	2002-2006	2006-2010	2010-2013	2013-2015	2015-2017	2017-2019	2019-2021	2021-2023	Estimated accuracy [m]
Hansbreen	2300	47	-24	-26	-[6]	-47[7]	-103	-260	-50	-95	-365	±45
Paierlbreen	4600	18	-100	-183	-100	-167	-250	-500	-100	-200	-425	±15
Mühlbacherbreen	2200	23	-53	-108	-158	-200	-160	-100	55	30	-150	±35
Storbreen	6700	-177	-186	-208	-250	-230	-235	-450	-200	-215	-240	±19
Hornbreen	4600	-57	-164	-238	-170	-183	-175	-115	-243	75	-365	±24
Svalisbreen	1700	-67	-79	-90	45	-233	-108	60	140	-30	-150	±39
Mendeleevbreen	2700	-33	209	-200	-275	-253	-200	-220	38	-30	-135	±45
Samarinbreen	3900	-33	-61	-106	-35	-83	-160	-190	-235	-100	-290	±48
Körberbreen	900	-20	-17	23	15	-50	-55	-45	-50	-60	-100	±17

Tab. 8 presents the average values of the indices calculated for the studied group of glaciers over the analysed time period (1992–2023). Although no single variable exhibits a perfectly linear trend, several glaciers—including Storbreen, Hansbreen, and Hornbreen how a consistent retreat trend,which is reflected in steadily decreasing CfD values. However, there is a noticeable increase in average front length (*Lc*) values between 2006 and 2019, with all averages exceeding 2.5 km. Simultaneously, circle diameters (*Dc*) were relatively high compared to other years, with values above 1.9 km. This was accompanied by relatively high values for both the ice-covered and ice-free areas.

In both 2021 and 2023, a decrease in the length of the fronts was observed, leading to a reduction in the size of both areas (*Ag* and *Ac*). Both indicators reflect glacier retreat, with *CfD* values below 0.5 and *CfE* exhibiting high values across all years of observation.

Prior to 2010, *CfD* values remained above 0.4, indicating less pronounced concavity in the frontal lines during this period. The decrease in CfD values suggests a shift toward more concave glacier fronts, indicating increased melting and structural instability. Meanwhile, the consistently high CfE values

[6] Due to high cloud cover the analysis for 2010 has not been conducted

[7] The average was determined in this case for the years 2006 - 2013

reflect ongoing frontal dynamics, even in periods of apparent stability. An increase in concavity was observed after 2010, as values fell below 0.4. The *CfE* indicator suggests the least dynamic front lines between 2006 and 2019. However, its values generally oscillated around 0.8 throughout the study period.

Tab. 8. Average values of indicators calculated for the studied group of glaciers from 1992 to 2023

Year	*Lc* [km]	*Dc* [km]	*Ag* [km^2]	*Ac* [km^2]	*CfD*	*CfE*
1992	2.20	1.82	1.36	3.27	0.43	0.83
1995	2.45	1.91	1.38	3.57	0.40	0.81
2002	2.20	1.72	0.99	2.73	0.43	0.81
2006	2.67	2.01	1.45	3.74	0.46	0.77
2010	2.54	1.95	1.28	3.31	0.46	0.79
2013	2.95	1.95	1.01	3.35	0.33	0.72
2015	2.77	2.07	1.22	3.94	0.33	0.77
2017	2.89	2.02	1.06	3.71	0.37	0.76
2019	2.77	1.95	0.89	3.16	0.42	0.76
2021	2.29	1.74	0.77	2.73	0.39	0.81
2023	2.27	1.69	0.61	2.77	0.33	0.80

Several glaciers, including Mühlbacherbreen, Samarinbreen, and Körberbreen, exhibit notable stability in the observed indicator values. However, as noted above, these values indicate a systematic retreat. In contrast, other glaciers, such as Storbreen, Hansbreen, and Hornbreen, display a linear trend of increasing retreat, reflected in a steady decline in *CfD* values. The characteristics of other glaciers are discussed in greater detail in the following section.

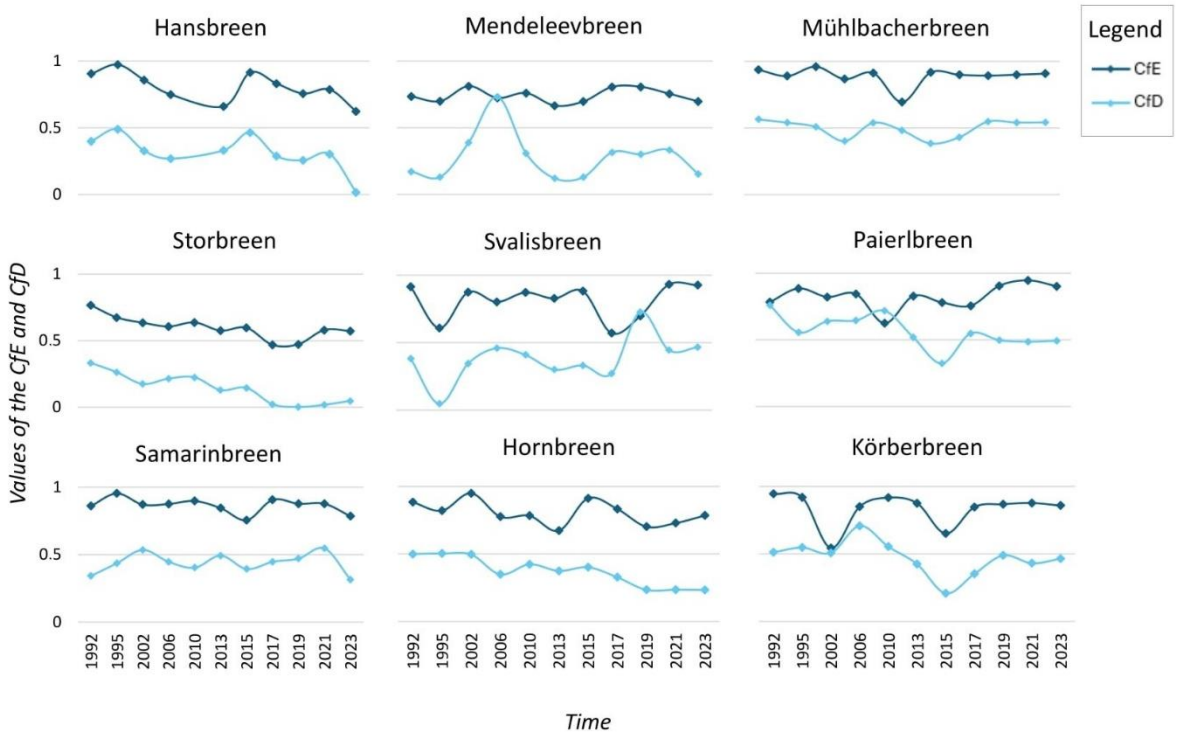

Fig. 7. Comparison of CfE and CfD indicators for selected glaciers from 1992 to 2023

6. DISCUSSION

The analysis of glacier front changes in the Hornsund Fjord over the period 1992–2023 reveals a clear overall trend of retreat among all studied glaciers, though the rate and nature of this retreat vary significantly between individual cases. Some glaciers, such as Storbreen and Hansbreen, exhibit a consistent and accelerated recession, while others, like Mendeleevbreen and Svalisbreen, display more complex behavior including surge episodes and temporary advances. This variability highlights the influence of local topography, glaciological dynamics, and short-term climatic fluctuations on glacier response. The average annual retreat rates—from as low as 12 m/year to over 79 m/year—underscore both the spatial heterogeneity and the accelerating pace of glacier change in the region.

The collected data demonstrate the most intense dynamics of phenomena on the glaciers Svalisbreen, Mendeleevbreen and Paierlbreen. A graph showing the differences in *CfD* and *CfE* ratios was prepared for these glaciers, along with a comparison to Mühlbacherbreen, as presented in Fig. 8. Based on the location of the glaciers in a specific quadrant of the graph, conclusions about their current state can be drawn in accordance with Tab. 3.

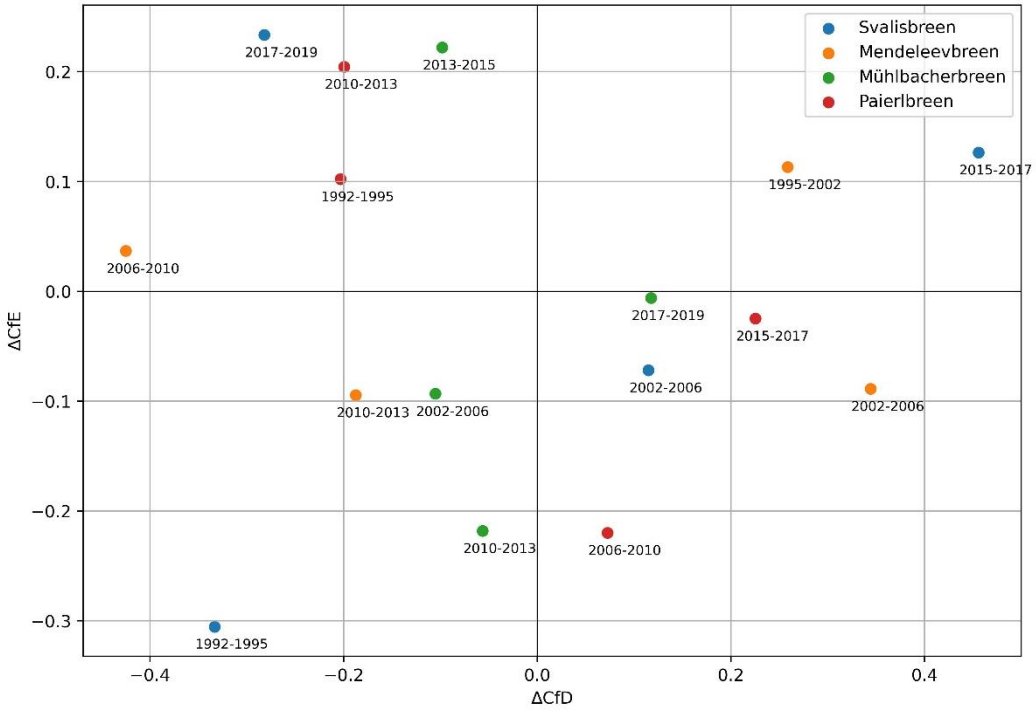

Fig. 8. Relationship between changes in ΔCfE and ΔCfD indicators for selected glaciers across successive periods

A clear increase in CfD values was noted after 2000 for Mendeleevbreen (Fig. 8), which is also confirmed by the observations presented in Table 7, where a glacial surge was recorded during this period. During this surge, the glacier was positioned in the first quadrant of the graph in Fig. 8, indicating simultaneous advance in glacier front distance (ΔCfD > 0) and elevation (ΔCfE > 0). This behavior is consistent with surge dynamics and has also been documented in previous studies [44] [45]. Following this episode, a marked shift in trend occurred - Mendeleevbreen transitioned toward the third and fourth quadrants, reflecting renewed retreat and thinning, with an average recession rate reaching

approximately 250 meters per year, as supported by our data (Table 7, Figs. 7 and 8) and corroborated by other sources [23] [46].

A similar transitional pattern was observed for Svalisbreen, which showed a significant increase in both CfD and CfE after 2015, placing the glacier in the first quadrant of Fig. 8. This corresponds to the recorded frontal advance between 2015 and 2019 (Table 7), suggesting localized thickening and forward movement. Previously, between 1992 and 1995, Svalisbreen had been situated in the third quadrant, indicating simultaneous retreat and thinning, followed by a shift to the second quadrant (2002–2006), where a modest frontal retreat was paired with slight elevation gain. After the post-2015 surge, the glacier entered the fourth quadrant (2017–2019), characterized by horizontal retreat despite elevation gain, likely marking a transition toward retreat following temporary thickening. The occurrence of surge-type dynamics on Svalisbreen has also been substantiated in the literature [39] [47].

In contrast, Paierlbreen showed consistent retreat throughout the observation period, though the intensity of retreat varied across time. The glacier reached its maximum retreat rate between 2015 and 2017, averaging around 500 meters per year (Table 7), which aligns with the elevated index values observed in Fig. 7. Notably, during this peak retreat phase, Paierlbreen occupied the second quadrant in Fig. 8—indicative of moderate retreat in distance with slight elevation gain, and substantially more intense than its retreat in previous periods. The shifting quadrant positions reflect changes in the magnitude but not the direction of glacial dynamics.

Mühlbacherbreen exhibited its most substantial retreat between 2006 and 2015, with rates ranging from 150 to 200 meters per year (Table 7). During this time, the glacier was located predominantly in the third and fourth quadrants of Fig. 8, signaling combined frontal retreat and thinning. However, in the period from 2017 to 2021, Mühlbacherbreen underwent a minor advance averaging 20–50 meters per year, and its position shifted to the boundary between the first and second quadrants—suggesting a halt in retreat and localized frontal thickening. Despite this positive change, the index values and quadrant location do not provide strong evidence of a glacier surge. Compared to Mendeleevbreen and Svalisbreen, the magnitude of frontal advance was significantly lower, implying that Mühlbacherbreen's response was less dynamic and potentially driven by different internal or external factors.

A unique case, discussed separately, involves observations of Chomjakovbreen based on satellite imagery. This glacier is located in a steep and narrow valley. Jania [48], based on research conducted in the 1980s, characterised Chomjakovbreen as a glacier that previously experienced surge phenomena. The results obtained for Chomjakovbreen are shown in Fig. 9. At the beginning of the observations (1992–2013), the glacier front shape remained relatively constant and was characterised by convexity. However, since 2015, the glacier front line has undergone rapid changes. It has become longer and more irregular in shape. Both *CfD* values and, after 2019, *CfE* values increased, confirming the high complexity of the glacier front line (Fig. 9b).

Additionally, the course generated for the most recent date (2023) deviates significantly from earlier front line positions. In Fig. 9a, the background is an RGB image from 2023. This image clearly shows that the shadow boundary was misidentified as the glacier front, rather than its actual position. Despite applying DOS1 (Dark Object Subtraction) atmospheric correction, the automatic generation of the Chomjakovbreen glacier front did not fully align with the actual front position. Earlier identified front lines (from 2013 onwards) were also affected by shadowing, a result of the aforementioned narrow valley and sharp slopes. The findings of this study unequivocally demonstrate a consistent pattern of glacial retreat across all examined sites. While CfD increases often align with surge events, CfE fluctuations highlight irregular front-line changes, possibly linked to internal glacier dynamics or external climatic influences. However, the magnitude and dynamics of this retreat exhibit notable variability, largely influenced by site-specific environmental conditions. To enhance the reliability of future assessments, it is recommended that advanced atmospheric correction techniques be employed

and that high-resolution, multi-angle satellite imagery be integrated to mitigate classification errors arising from shadowing effects.

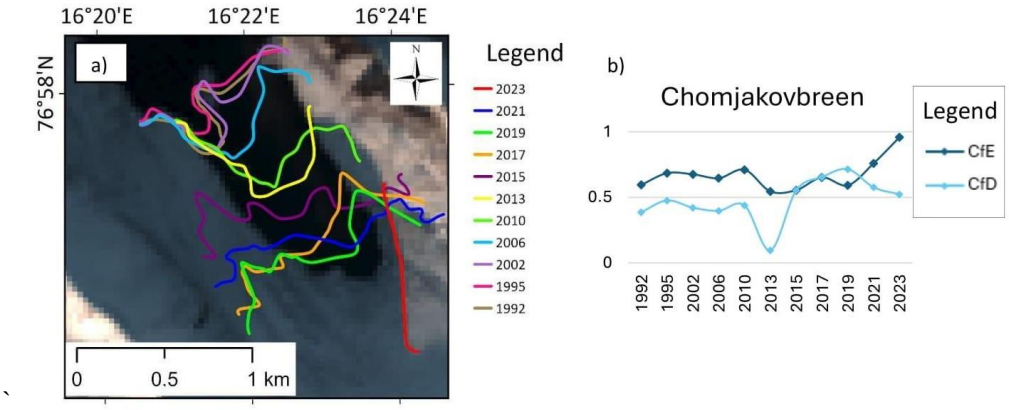

Fig. 9. Changes in the geometry of the Chomjakovbreen glacier front from 1992 to 2013 and the values of the CfE and CfD indicators

Additionally, the results of this study were compared with the observations presented by Błaszczyk et al. [23] and Dudek & Petlicki [49]. According to Błaszczyk et al. [23], for example, the advance rate of the Mendeleevbreen glacier front was approximately 220 m per year between 1995 and 2002. In the context of our results, this value is comparable, amounting to ~209 m per year. Similar temporal stages of surge and subsequent retreat were also observed for this glacier (Fig.8). Furthermore, the analysis by Dudek and Petlicki [49] reveals a general reduction in glacier area of approximately 16% between 1961 and 2010, as well as an acceleration in the rate of ice loss after 1990 (from 0.85 to 1.05 km²/ yr), indicating an intensification of ablation processes. These findings confirm the trend of accelerated glacier retreat in polar regions. In addition, structural lowering—up to 120 m in the case of tidewater glaciers—complements the picture of rapid three-dimensional changes in glacier morphology, which aligns with our own observations.

One limitation of the dataset is the temporal variability of satellite image acquisition dates, ranging from July to September. Since glacier front positions can change substantially during the ablation season, this variability may affect the comparability of CfE and CfD values between years. Although this reflects constraints in cloud-free image availability, it introduces a degree of uncertainty into the interpretation of annual retreat and advance rates.

7. CONCLUSIONS

The analysis of the results clearly indicates a significant retreat of glaciers in all studied cases during the investigated period, with the dynamics of this process varying according to local conditions. The overall dynamics of the Hornsund glaciers reveal the diversity of their behavior and responses to changing environmental conditions. Some glaciers exhibit a rapid, permanent retreat, leading to their accelerated degradation, while others experience additional surge phenomena. This variability underscores the importance of continued monitoring to better understand the mechanisms driving these changes. Importantly, these results are consistent with global patterns of glacial retreat, further reinforcing the connection between glacier behavior and broader climate change.

The integration of segmentation methods based on satellite imagery and the automated processing of subsequent datasets offers a comprehensive approach to monitoring the position of glacier fronts. The

CfD and CfE indices have proven to be effective tools for analyzing changes in glacier fronts, capturing both long-term climate trends and short-term fluctuations. These indices represent not only the physical changes in glacier fronts but also the broader mechanisms governing glacial dynamics. Notably, significant increases in CfD values indicate the occurrence of glacial surge phenomena, providing valuable insights into these episodic events.

REFERENCES

1. Zemp, M, et al. 2019. Global glacier mass changes and their contributions to sea-level rise from 1961 to 2016. *Nature* **568**, 382–386.
2. Niewiadomski, J 1982. Report on the activities of the research expedition of the Polish Academy of Sciences to Spitsbergen 1980/1981. *Polish Polar Research* **3**, 123-127.
3. Andreassen, LM, Elvehøy, H and Kjøllmoen, B 2002. Using aerial photography to study glacier changes in Norway. *Annals of Glaciology* **34**, 343–348. doi:10.3189/172756402781817626
4. Gao, J and Liu, Y 2001. Applications of remote sensing, GIS and GPS in glaciology: a review. *Progress in Physical Geography* **25,** 520 - 540. Accessed: 15.07.2025r. https://api.semanticscholar.org/CorpusID:14483397
5. Cielos, RR, et al. 2016. Geomatic methods applied to the study of the front position changes of Johnsons and Hurd Glaciers, Livingston Island, Antarctica, between 1957 and 2013. *Earth System Science Data* **8(2),** 341–353. https://doi.org/10.5194/essd-8-341-2016
6. Jóhannesson, T et al. 2013. Ice-volume changes, bias estimation of mass-balance measurements and changes in subglacial lakes derived by lidar mapping of the surface of Icelandic glaciers. *Annals of Glaciology* **54**, 63–74.
7. Engeset, R and Weydahl, DJ 1998. Analysis of glaciers and geomorphology on Svalbard using multitemporal ERS-1 SAR images. *IEEE Trans. Geosci. Remote. Sens.* **36**, 1879-1887. doi: 10.1109/36.729359
8. Schellenberger, T et al. 2015. Surface speed and frontal ablation of Kronebreen and Kongsbreen, NW Svalbard, from SAR offset tracking. *The Cryosphere* **9**, 2339–2355. https://doi.org/10.5194/tc-9-2339-2015.
9. Strozzi, T et al. 2002. Glacier motion estimation using SAR offset-tracking procedures. *IEEE Transactions on Geoscience and Remote Sensing* **40**, 2384–2391. doi: 10.1109/TGRS.2002.805079
10. Wen, M and Wang, T 2025. Review of SAR imaging geodesy for glacier velocity monitoring. *Geodesy and Geodynamics* **16(3),** 262–274. https://doi.org/10.1016/j.geog.2024.08.004
11. Friedl, P, Seehaus, T and Braun, M 2021. Global time series and temporal mosaics of glacier surface velocities, derived from Sentinel-1 data. *Earth System Science Data*. https://doi.org/10.5194/essd-2021-106
12. Paul, F, Huggel, C and Kääb, A 2004. Combining satellite multispectral image data and a digital elevation model for mapping debris-covered glaciers. *Remote Sensing of Environment* **89(4),** 510–518. https://doi.org/10.1016/j.rse.2003.11.007
13. Racoviteanu, AE, Williams, MW and Barry, RG 2008. Optical Remote Sensing of Glacier Characteristics: A Review with Focus on the Himalaya. *Sensors* **8(5),** 3355-3383. https://doi.org/10.3390/s8053355
14. Arigony-Neto, J et al. 2014. Monitoring Glacier Changes on the Antarctic Peninsula, in: Kargel, JS, Leonard, GJ, Bishop, MP, Kääb, A, Raup, BH (Eds.), *Global Land Ice Measurements from Space*. Springer, Berlin, Heidelberg, pp. 717–741.
15. Paul, F et al. 2002. The new remote-sensing-derived Swiss glacier inventory: I. Methods. Annals of Glaciology **34**, 355–361. https://doi.org/10.3189/172756402781817941

16. Frey, H, Paul, F and Strozzi, T, 2012. Compilation of a glacier inventory for the western Himalayas from satellite data: Methods, challenges, and results. *Remote Sensing of Environment* **124**, 832–843. https://doi.org/10.1016/j.rse.2012.06.020
17. Paul, F et al. 2013. On the accuracy of glacier outlines derived from remote-sensing data. *Annals of Glaciology*, 54(63), 171–182. doi:10.3189/2013AoG63A296
18. Baumhoer, CA, Dietz, AJ, Dech, S and Kuenzer, C 2018. Remote Sensing of Antarctic Glacier and Ice-Shelf Front Dynamics—A Review. *Remote Sensing* **10(9),** 1445. https://doi.org/10.3390/rs10091445
19. Sood, S et al. 2022. Mapping Samudra Tapu glacier: A holistic approach utilizing radar and optical remote sensing data for glacier radar facies mapping and velocity estimation. Advances in Space Research **70(12),** 3975–3999. https://doi.org/10.1016/j.asr.2022.10.030
20. Vieli, A, Jania, J and Kolondra, L 2002. The retreat of a tidewater glacier: observations and model calculations on Hansbreen, Spitsbergen. *Journal of Glaciology* **48(163),** s. 592–600. doi:10.3189/172756502781831089.
21. Strozzi, T, Kääb, A and Schellenberger, T 2017. Frontal destabilization of Stonebreen, Edgeøya, Svalbard. *The Cryosphere* **11**, 553–566. https://doi.org/10.5194/tc-11-553-2017
22. Rees, WG and Arnold, NS 2007. Mass balance and dynamics of a valley glacier measured by high-resolution LiDAR, *Polar Record* **43(4),** pp. 311–319. doi:10.1017/S0032247407006419.
23. Błaszczyk, M, Jania, JA, Kolondra, L 2013. Fluctuations of tidewater glaciers in Hornsund Fjord (Southern Svalbard) since the beginning of the 20th century. *Polish Polar Research* **34**, 327–352.
24. Ciepły, M, Ignatiuk, D, Moskalik, M et al. 2023. Seasonal changes in submarine melting mechanisms controlling frontal ablation of Hansbreen, Svalbard. *Journal of Glaciology* **69(278),** 1886-1899. doi:10.1017/jog.2023.69
25. Hagen, JO et al. 2003. Glaciers in Svalbard: mass balance, runoff and freshwater flux. *Polar Research* **22**, 145–159.
26. Hagen, JO 1993. *Glacier Atlas of Svalbard and Jan Mayen*. Oslo: Norsk Polarinstitutt.
27. Strzelecki, MC et al. 2020. New fjords, new coasts, new landscapes: The geomorphology of paraglacial coasts formed after recent glacier retreat in Brepollen (Hornsund, southern Svalbard). *Earth Surface Processes and Landforms* **45**, 1325–1334.
28. Ziaja, W, Ostafin, K 2015. Landscape-seascape dynamics in the isthmus between Sørkapp Land and the rest of Spitsbergen : Will a new big Arctic island form? *AMBIO* **44(4).** https://doi.org/10.1007/s13280-014-0572-1
29. Jenkins, S 2022. Is Anthropogenic Global Warming Accelerating? *Journal of Climate* **35(24),** 7873-7890. https://doi.org/10.1175/JCLI-D-22-0081.1
30. Wawrzyniak, T, Osuch, M 2020. A 40-year High Arctic climatological dataset of the Polish Polar Station Hornsund (SW Spitsbergen, Svalbard). *Earth System Science Data* **12**, 805–815.
31. Błaszczyk, M et al. 2019. Freshwater input to the Arctic fjord Hornsund (Svalbard). *Polar Research* **38.**
32. Hall, DK, Riggs, GA and Salomonson, VV 1995. Development of methods for mapping global snow cover using Moderate Resolution Imaging Spectroradiometer (MODIS) data. *Remote Sensing of Environment* **54(2),** 127–140. https://doi.org/10.1016/0034-4257(95)00137-P
33. Keshri, AK, Shukla, A, Gupta, RP 2009. ASTER ratio indices for supraglacial terrain mapping. *International Journal of Remote Sensing* **30,** 519–524.
34. Zhang, Y and Tsinghua University Press 2017. *Image Engineering. Vol 2, Image Analysis* (1st ed.). De Gruyter, https://doi.org/10.1515/9783110524123

35. MacKay, DJC 2003. *Information Theory, Inference and Learning Algorithms*, Cambridge: Cambridge University Press.
36. Ahmed, M, Seraj, R and Islam, SMS 2020. The k-means Algorithm: A Comprehensive Survey and Performance Evaluation. *Electronics* **9(8),** 1295. https://doi.org/10.3390/electronics9081295
37. Wacker, AG, Landgrebe, DA 1972. *Minimum distance classification in remote sensing.* Presented at the Canadian Symposium for Remote Sensing, 7-9 February 1972, Ottawa.
38. Camps-Valls, G 2009. *Machine learning in remote sensing data processing*, 2009 IEEE International Workshop on Machine Learning for Signal Processing, *IEEE*, Grenoble, France, 1-4 September 2009, 1–6.
39. Szafraniec, JE 2020. Ice-Cliff Morphometry in Identifying the Surge Phenomenon of Tidewater Glaciers (Spitsbergen, Svalbard). *Geosciences* **10**, 328.
40. Richards, JA 2013. *Remote sensing digital image analysis: An introduction (5th ed.)*. Springer. https://doi.org/10.1007/978-3-642-30062-2. Access: 28.05.2025r.
41. Mountrakis, G, Im, J and Ogole, C 2011. Support vector machines in remote sensing: A review. *ISPRS Journal of Photogrammetry and Remote Sensing* **66(3),** 247–259. https://doi.org/10.1016/j.isprsjprs.2010.11.001
42. Belgiu, M and Drăguţ, L 2016. Random forest in remote sensing: A review of applications and future directions. *ISPRS Journal of Photogrammetry and Remote Sensing* **114,** 24–31. https://doi.org/10.1016/j.isprsjprs.2016.01.011
43. Esri 2025. UpdateCursor class. ArcGIS Pro Documentation. Accessed: 05.06.2025r. https://pro.arcgis.com/en/pro-app/latest/arcpy/data-access/updatecursor-class.htm
44. Błaszczyk, M, Jania, JA, Hagen, JO 2009. Tidewater glaciers of Svalbard: Recent changes and estimates of calving fluxes. *Polish Polar Research* **30**, 85-142.
45. Sund, M, Eiken, T, Rolstad Denby, C 2011. Velocity structure, front position changes and calving of the tidewater glacier Kronebreen, Svalbard. *The Cryosphere Discussions* **5,** 41–73.
46. Moskalik, M, Błaszczyk, M, Jania, J 2014. Statistical analysis of Brepollen bathymetry as a key to determine average depths on a glacier foreland. *Geomorphology* **206**, 262–270.
47. Błaszczyk, M et al. 2023. The Response of Tidewater Glacier Termini Positions in Hornsund (Svalbard) to Climate Forcing, 1992–2020. *Journal of Geophysical Research: Earth Surface* **128**, e2022JF006911.
48. Jania, J 1988. *Dynamiczne procesy glacjalne na południowym Spitzbergenie: w świetle badań fotointerpretacyjnych i fotogrametrycznych* [Dynamic glacial processes in southern Spitsbergen: in the light of photointerpretation and photogrammetric studies]. Katowice: Wydawnictwo Uniwersytetu Śląskiego.
49. Dudek, J and Pętlicki, M 2023. Unlocking archival maps of the Hornsund fjord area for monitoring glaciers of the Sørkapp Land peninsula, Svalbard. *Earth System Science Data* **15(9),** 3869–3889. https://doi.org/10.5194/essd-15-3869-2023